

Supporting information

Successive constructions of regular tetra-, hexa- and octanuclear microporous polyoxovanadates(III) for gas adsorptions

Zhen-Lang Xie, Dong-Li An, Wei-Zheng Weng, Zhao-Hui Zhou*

*State Key Laboratory of Physical Chemistry of Solid Surfaces and Department of Chemistry, College of Chemistry and Chemical Engineering, Xiamen University, Xiamen, 361005, China, Tel: + 86-592-2184531; Fax: + 86-592-2183047
zhzhou@xmu.edu.cn*

Figures and Table Options

Figure S1. Ball-and-stick models of polyanionic cluster $[V_4(\mu_2\text{-OH})_4(\text{ox})_4(\text{pz})_4]^{4-}$ (1).	3
Figure S2. (a) "Violet" and (b) "yellow": cosine-like "V–O–S–O–V–O" rings of 4 . (c): sinusoid-like "V–N–N–V" ring.	4
Figure S3. 2D packing diagram of 1 observed along the <i>c</i> axis.	5
Figure S4. Channels in 4 viewed along <i>b</i> axis.	6
Figure S5. Fourier transform infrared (FT-IR) spectra of $(\text{NH}_4)_2\text{K}_2[V_4(\mu_2\text{-OH})_4(\text{ox})_4(\text{pz})_4]\cdot 9\text{H}_2\text{O}$ (1), $(\text{NH}_4)_2\text{Na}_2[V_4(\mu_2\text{-OH})_4(\text{ox})_4(4\text{-mpz})_4]\cdot 7\text{H}_2\text{O}$ (2), $\text{K}_2[V_6(\mu_2\text{-OH})_6(\text{ox})_6(\text{Hdatrz})_6]\text{Cl}_2\cdot 29.5\text{H}_2\text{O}$ (3) and $[V_8(\mu_2\text{-OH})_8(\text{SO}_3)_8(\text{Hdatrz})_8]\cdot 38\text{H}_2\text{O}$ (4).	7
Figure S6. Solid-state UV-vis spectra of $(\text{NH}_4)_2\text{K}_2[V_4(\mu_2\text{-OH})_4(\text{ox})_4(\text{pz})_4]\cdot 9\text{H}_2\text{O}$ (1), $(\text{NH}_4)_2\text{Na}_2[V_4(\mu_2\text{-OH})_4(\text{ox})_4(4\text{-mpz})_4]\cdot 7\text{H}_2\text{O}$ (2), $\text{K}_2[V_6(\mu_2\text{-OH})_6(\text{ox})_6(\text{Hdatrz})_6]\text{Cl}_2\cdot 29.5\text{H}_2\text{O}$ (3) and $[V_8(\mu_2\text{-OH})_8(\text{SO}_3)_8(\text{Hdatrz})_8]\cdot 38\text{H}_2\text{O}$ (4).	8
Figure S7. TGA curves of solid samples $(\text{NH}_4)_2\text{K}_2[V_4(\mu_2\text{-OH})_4(\text{ox})_4(\text{pz})_4]\cdot 9\text{H}_2\text{O}$ (1 , a), $(\text{NH}_4)_2\text{Na}_2[V_4(\mu_2\text{-OH})_4(\text{ox})_4(4\text{-mpz})_4]\cdot 7\text{H}_2\text{O}$ (2 , b), $\text{K}_2[V_6(\mu_2\text{-OH})_6(\text{ox})_6(\text{Hdatrz})_6]\text{Cl}_2\cdot 29.5\text{H}_2\text{O}$ (3 , c) and $[V_8(\mu_2\text{-OH})_8(\text{SO}_3)_8(\text{Hdatrz})_8]\cdot 38\text{H}_2\text{O}$ (4 , d).	9
Figure S8. Temperature dependence of magnetic susceptibilities of $(\text{NH}_4)_2\text{K}_2[V_4(\mu_2\text{-OH})_4(\text{ox})_4(\text{pz})_4]\cdot 9\text{H}_2\text{O}$ (1 , a), $(\text{NH}_4)_2\text{Na}_2[V_4(\mu_2\text{-OH})_4(\text{ox})_4(4\text{-mpz})_4]\cdot 7\text{H}_2\text{O}$ (2 , b), $\text{K}_2[V_6(\mu_2\text{-OH})_6(\text{ox})_6(\text{Hdatrz})_6]\text{Cl}_2\cdot 29.5\text{H}_2\text{O}$ (3 , c) and $[V_8(\mu_2\text{-OH})_8(\text{SO}_3)_8(\text{Hdatrz})_8]\cdot 38\text{H}_2\text{O}$ (4 , d) under 0.1 T applied field between 300 and 2 K. Blue lines correspond to the best fitting results.	10
Figure S9. N_2 adsorption-desorption isotherms of $(\text{NH}_4)_2\text{K}_2[V_4(\mu_2\text{-OH})_4(\text{ox})_4(\text{pz})_4]\cdot 9\text{H}_2\text{O}$ (1), $(\text{NH}_4)_2\text{Na}_2[V_4(\mu_2\text{-OH})_4(\text{ox})_4(4\text{-mpz})_4]\cdot 7\text{H}_2\text{O}$ (2) and $[V_8(\mu_2\text{-OH})_8(\text{SO}_3)_8(\text{Hdatrz})_8]\cdot 38\text{H}_2\text{O}$ (4) at 77K.	11

Figure S10. (a) CO ₂ adsorption isotherms for 1 , 2 and 4 at 288 K; (b) Isostatic heat of adsorption (Q_{st}) plotted against CO ₂ uptake for 1 , 2 and 4	12
Figure S11. IAST selectivity of equimolar CO ₂ /CH ₄ = 0.5/0.5 mixture for 4	13
Figure S12. Comparison of the observed PXRD (red) with the simulated patterns (black) calculated from the SXRD data for (NH ₄) ₂ K ₂ [V ₄ (μ ₂ -OH) ₄ (ox) ₄ (pz) ₄]·9H ₂ O (1 , a), (NH ₄) ₂ Na ₂ [V ₄ (μ ₂ -OH) ₄ (ox) ₄ (4-mpz) ₄]·7H ₂ O (2 , b), K ₂ [V ₆ (μ ₂ -OH) ₆ (ox) ₆ (Hdatrz) ₆]Cl ₂ ·29.5H ₂ O (3 , c) and [V ₈ (μ ₂ -OH) ₈ (SO ₃) ₈ (Hdatrz) ₈]·38H ₂ O (4 , d), respectively.....	14
Table S1. Crystallographic data and structural refinement details for (NH ₄) ₂ K ₂ [V ₄ (μ ₂ -OH) ₄ (ox) ₄ (pz) ₄]·9H ₂ O (1), (NH ₄) ₂ Na ₂ [V ₄ (μ ₂ -OH) ₄ (ox) ₄ (4-mpz) ₄]·7H ₂ O (2), K ₂ [V ₆ (μ ₂ -OH) ₆ (ox) ₆ (Hdatrz) ₆]Cl ₂ ·29.5H ₂ O (3) and [V ₈ (μ ₂ -OH) ₈ (SO ₃) ₈ (Hdatrz) ₈]·38H ₂ O (4), respectively.....	15
Table S2. Selected bond distances (Å) and angles (°) for (NH ₄) ₂ K ₂ [V ₄ (μ ₂ -OH) ₄ (ox) ₄ (pz) ₄]·9H ₂ O (1), (NH ₄) ₂ Na ₂ [V ₄ (μ ₂ -OH) ₄ (ox) ₄ (4-mpz) ₄]·7H ₂ O (2), K ₂ [V ₆ (μ ₂ -OH) ₆ (ox) ₆ (Hdatrz) ₆]Cl ₂ ·29.5H ₂ O (3) and [V ₈ (μ ₂ -OH) ₈ (SO ₃) ₈ (Hdatrz) ₈]·38H ₂ O (4), respectively.....	17
Table S3. Hydrogen bonds observed in (NH ₄) ₂ K ₂ [V ₄ (μ ₂ -OH) ₄ (ox) ₄ (pz) ₄]·9H ₂ O (1), (NH ₄) ₂ Na ₂ [V ₄ (μ ₂ -OH) ₄ (ox) ₄ (4-mpz) ₄]·7H ₂ O (2), K ₂ [V ₆ (μ ₂ -OH) ₆ (ox) ₆ (Hdatrz) ₆]Cl ₂ ·29.5H ₂ O (3) and [V ₈ (μ ₂ -OH) ₈ (SO ₃) ₈ (Hdatrz) ₈]·38H ₂ O (4).....	20
Table S4. Comparisons of V–O distances (Å) in 1 ~ 4 and a series of tetra-, hexa- and octanuclear vanadium(III/IV/V) clusters with bridging μ ₂ -hydroxy/μ ₂ -oxygen groups.	22
Table S5. Bond valence sum calculations for (NH ₄) ₂ K ₂ [V ₄ (μ ₂ -OH) ₄ (ox) ₄ (pz) ₄]·9H ₂ O (1), (NH ₄) ₂ Na ₂ [V ₄ (μ ₂ -OH) ₄ (ox) ₄ (4-mpz) ₄]·7H ₂ O (2), K ₂ [V ₆ (μ ₂ -OH) ₆ (ox) ₆ (Hdatrz) ₆]Cl ₂ ·29.5H ₂ O (3) and [V ₈ (μ ₂ -OH) ₈ (SO ₃) ₈ (Hdatrz) ₈]·38H ₂ O (4), respectively.....	24
Table S6. Comparisons of CO ₂ adsorption data for 1 , 2 and 4 with other porous polyoxometalates at 298 K.	25
Table S7. V–μ ₂ -O distances (Å) for (NH ₄) ₂ K ₂ [V ₄ (μ ₂ -OH) ₄ (ox) ₄ (pz) ₄]·9H ₂ O (1), (NH ₄) ₂ Na ₂ [V ₄ (μ ₂ -OH) ₄ (ox) ₄ (4-mpz) ₄]·7H ₂ O (2) and [V ₈ (μ ₂ -OH) ₈ (SO ₃) ₈ (Hdatrz) ₈]·38H ₂ O (4) before and after O ₂ adsorption.....	26

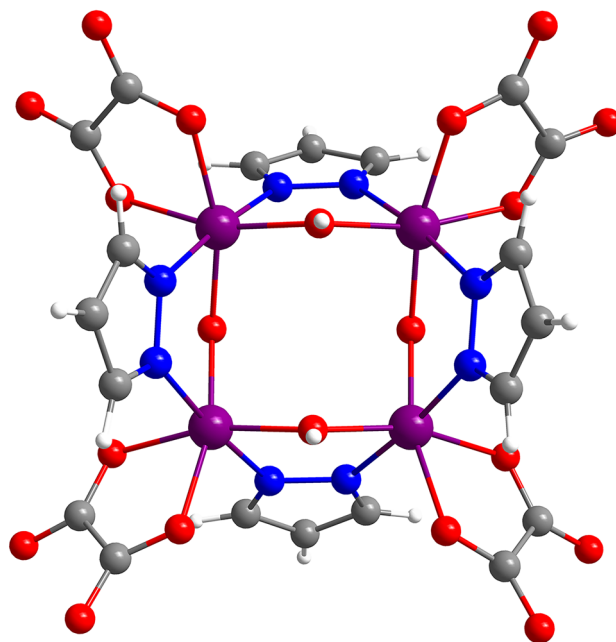


Figure S1. Ball-and-stick models of polyanionic cluster $[V_4(\mu_2\text{-OH})_4(\text{ox})_4(\text{pz})_4]^{4-}$ (**1**).

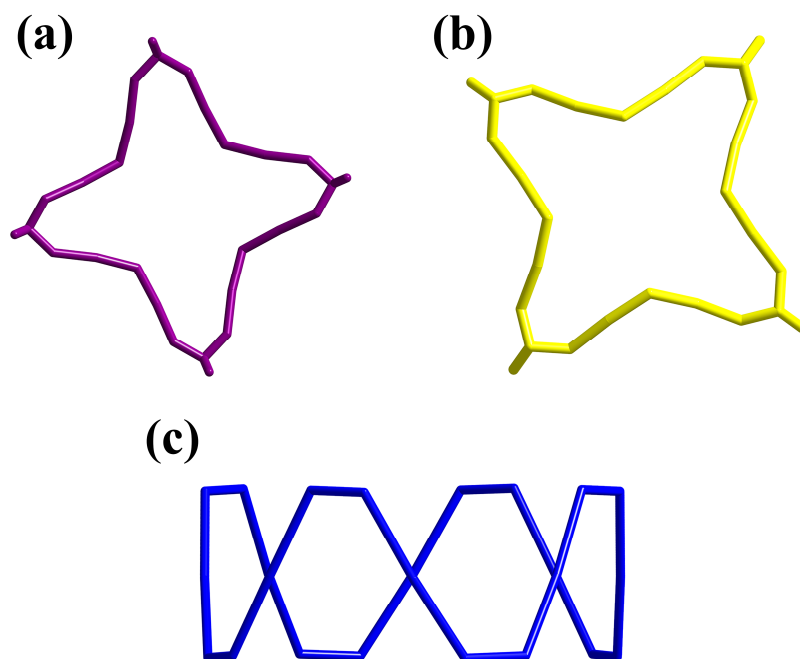


Figure S2. (a) "Violet" and (b) "yellow": cosine-like "V-O-S-O-V-O" rings of 4. (c): sinusoid-like "V-N-N-V" ring.

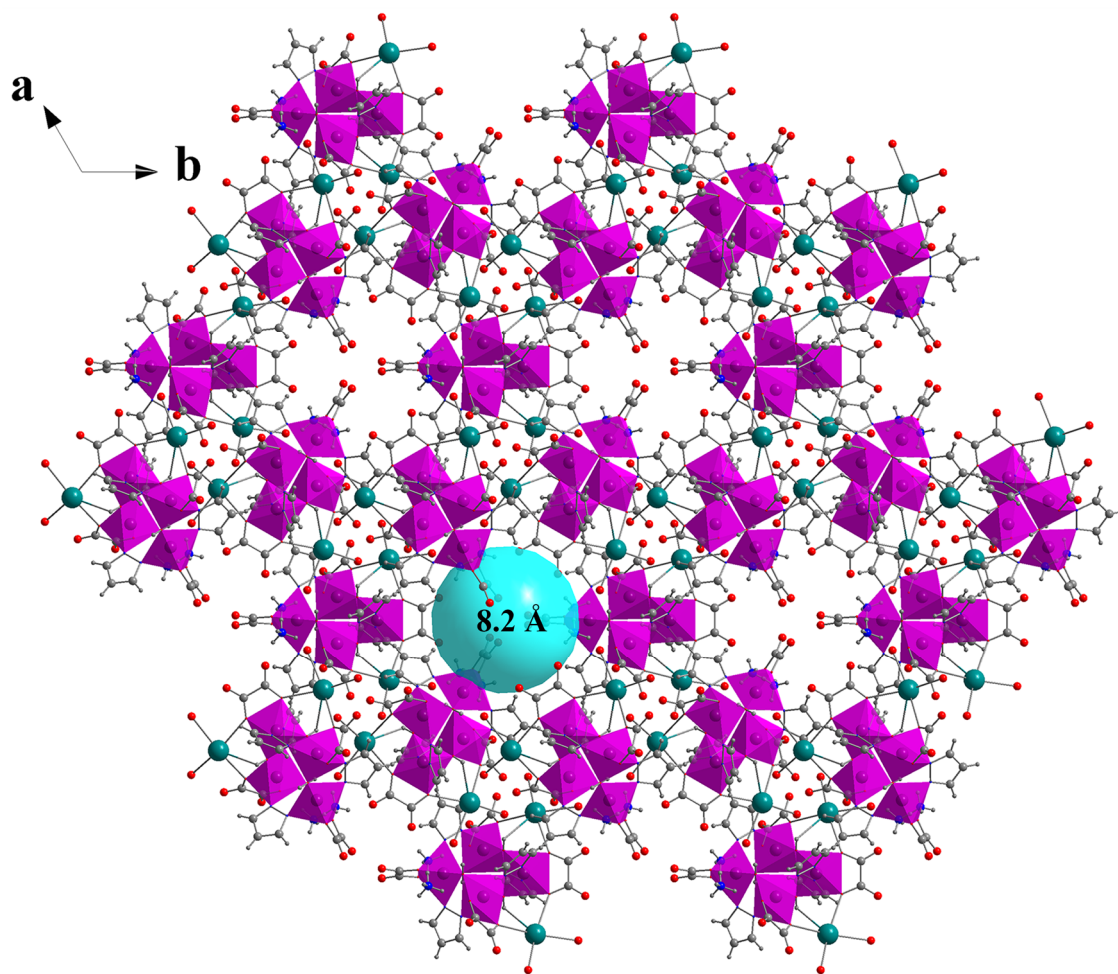


Figure S3. 2D packing diagram of **1** observed along the *c* axis.

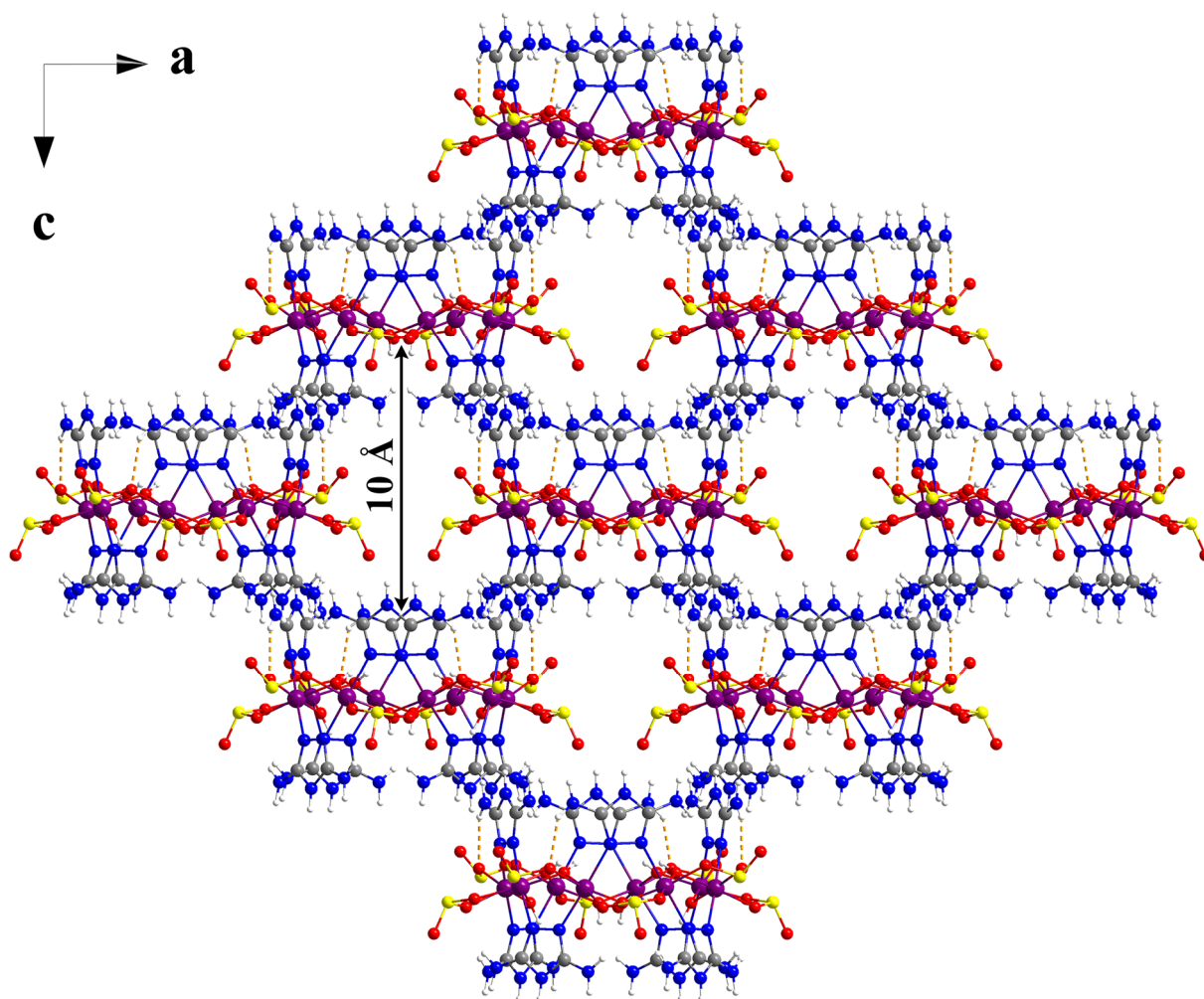


Figure S4. Channels in **4** viewed along b axis.

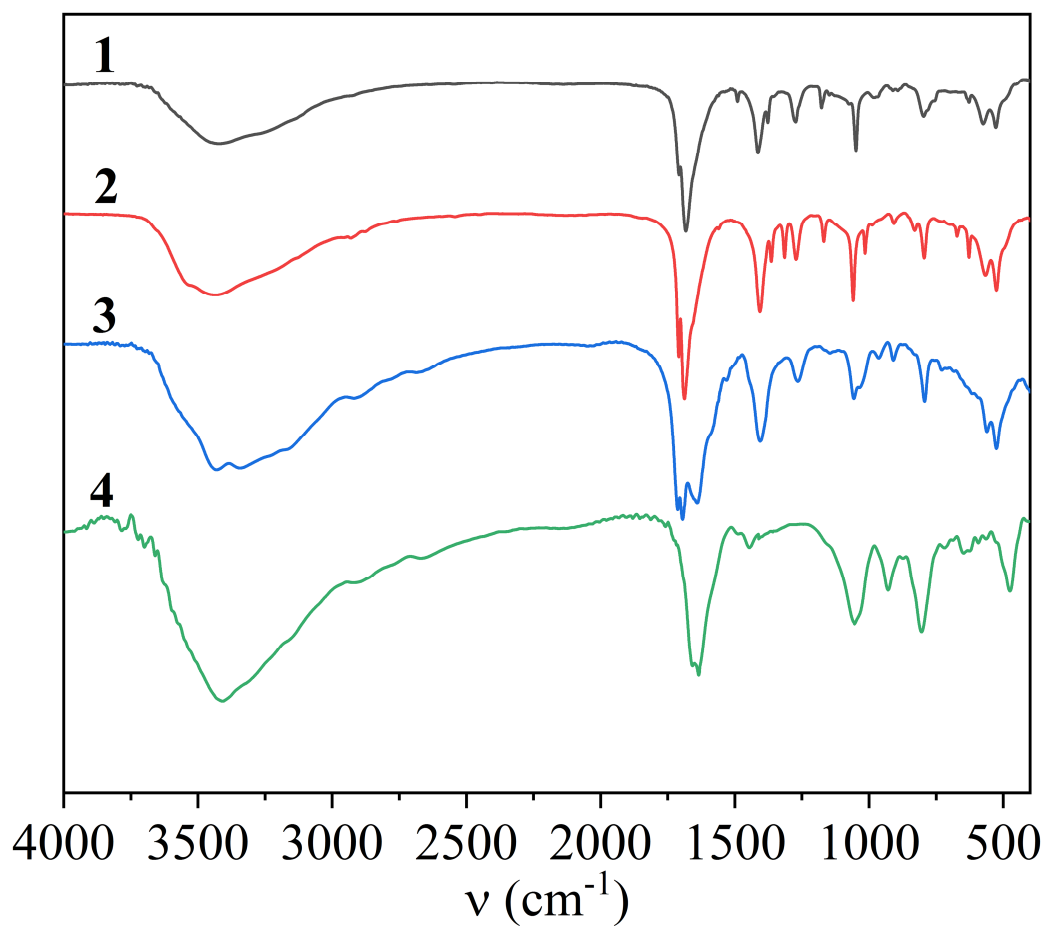


Figure S5. Fourier transform infrared (FT-IR) spectra of $(\text{NH}_4)_2\text{K}_2[\text{V}_4(\mu_2\text{-OH})_4(\text{ox})_4(\text{pz})_4]\cdot 9\text{H}_2\text{O}$ (**1**), $(\text{NH}_4)_2\text{Na}_2[\text{V}_4(\mu_2\text{-OH})_4(\text{ox})_4(4\text{-mpz})_4]\cdot 7\text{H}_2\text{O}$ (**2**), $\text{K}_2[\text{V}_6(\mu_2\text{-OH})_6(\text{ox})_6(\text{Hdatrz})_6]\text{Cl}_2\cdot 29.5\text{H}_2\text{O}$ (**3**) and $[\text{V}_8(\mu_2\text{-OH})_8(\text{SO}_3)_8(\text{Hdatrz})_8]\cdot 38\text{H}_2\text{O}$ (**4**).

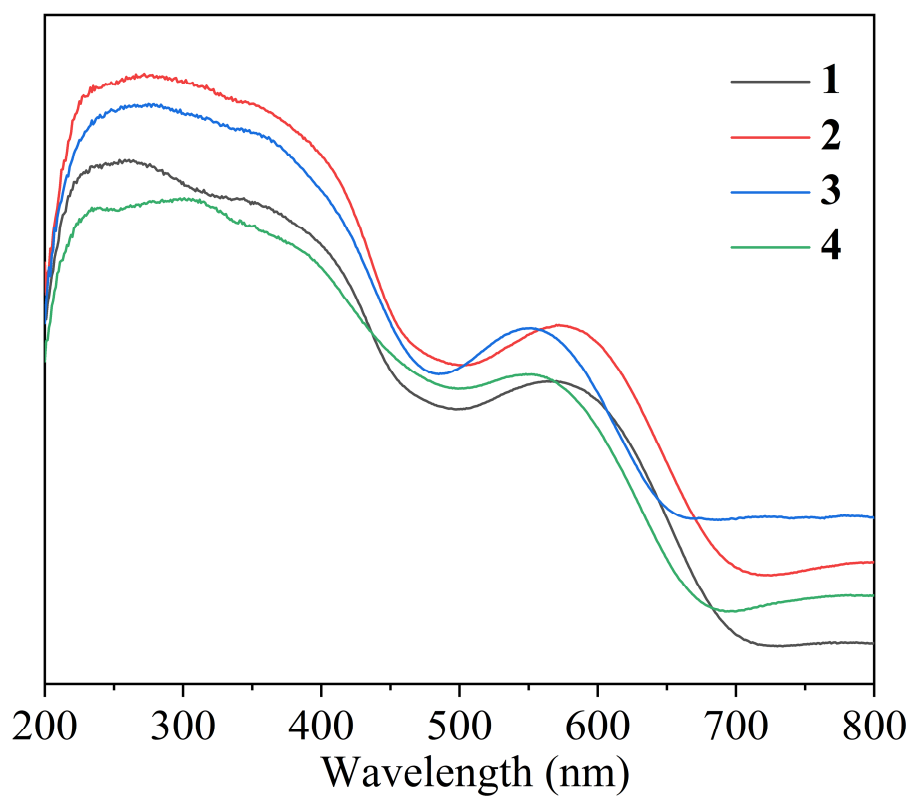


Figure S6. Solid-state UV-vis spectra of $(\text{NH}_4)_2\text{K}_2[\text{V}_4(\mu_2\text{-OH})_4(\text{ox})_4(\text{pz})_4]\cdot 9\text{H}_2\text{O}$ (**1**), $(\text{NH}_4)_2\text{Na}_2[\text{V}_4(\mu_2\text{-OH})_4(\text{ox})_4(4\text{-mpz})_4]\cdot 7\text{H}_2\text{O}$ (**2**), $\text{K}_2[\text{V}_6(\mu_2\text{-OH})_6(\text{ox})_6(\text{Hdatrz})_6]\text{Cl}_2\cdot 29.5\text{H}_2\text{O}$ (**3**) and $[\text{V}_8(\mu_2\text{-OH})_8(\text{SO}_3)_8(\text{Hdatrz})_8]\cdot 38\text{H}_2\text{O}$ (**4**).

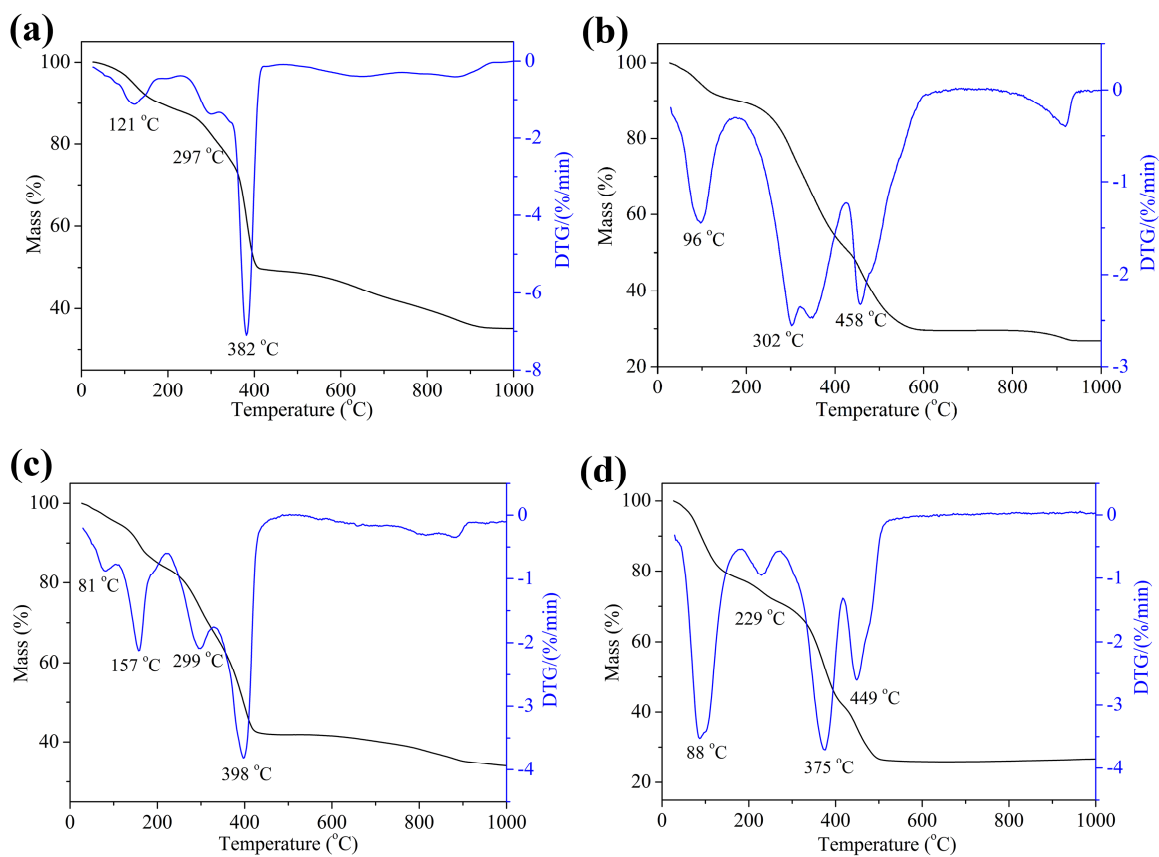


Figure S7. TGA curves of solid samples $(\text{NH}_4)_2\text{K}_2[\text{V}_4(\mu_2\text{-OH})_4(\text{ox})_4(\text{pz})_4]\cdot 9\text{H}_2\text{O}$ (**1**, a), $(\text{NH}_4)_2\text{Na}_2[\text{V}_4(\mu_2\text{-OH})_4(\text{ox})_4(4\text{-mpz})_4]\cdot 7\text{H}_2\text{O}$ (**2**, b), $\text{K}_2[\text{V}_6(\mu_2\text{-OH})_6(\text{ox})_6(\text{Hdatrz})_6]\text{Cl}_2\cdot 29.5\text{H}_2\text{O}$ (**3**, c) and $[\text{V}_8(\mu_2\text{-OH})_8(\text{SO}_3)_8(\text{Hdatrz})_8]\cdot 38\text{H}_2\text{O}$ (**4**, d).

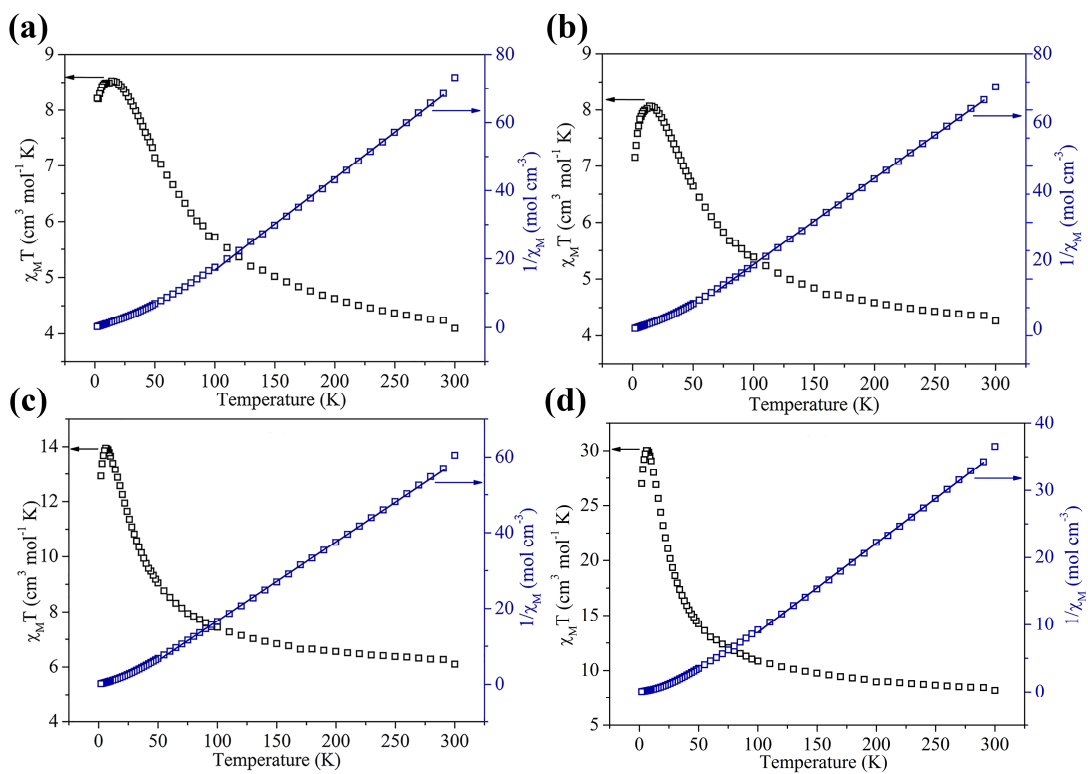


Figure S8. Temperature dependence of magnetic susceptibilities of $(\text{NH}_4)_2\text{K}_2[\text{V}_4(\mu_2\text{-OH})_4(\text{ox})_4(\text{pz})_4]\cdot 9\text{H}_2\text{O}$ (**1**, a), $(\text{NH}_4)_2\text{Na}_2[\text{V}_4(\mu_2\text{-OH})_4(\text{ox})_4(4\text{-mpz})_4]\cdot 7\text{H}_2\text{O}$ (**2**, b), $\text{K}_2[\text{V}_6(\mu_2\text{-OH})_6(\text{ox})_6(\text{Hdatrz})_6]\text{Cl}_2\cdot 29.5\text{H}_2\text{O}$ (**3**, c) and $[\text{V}_8(\mu_2\text{-OH})_8(\text{SO}_3)_8(\text{Hdatrz})_8]\cdot 38\text{H}_2\text{O}$ (**4**, d) under 0.1 T applied field between 300 and 2 K. Blue lines correspond to the best fitting results.

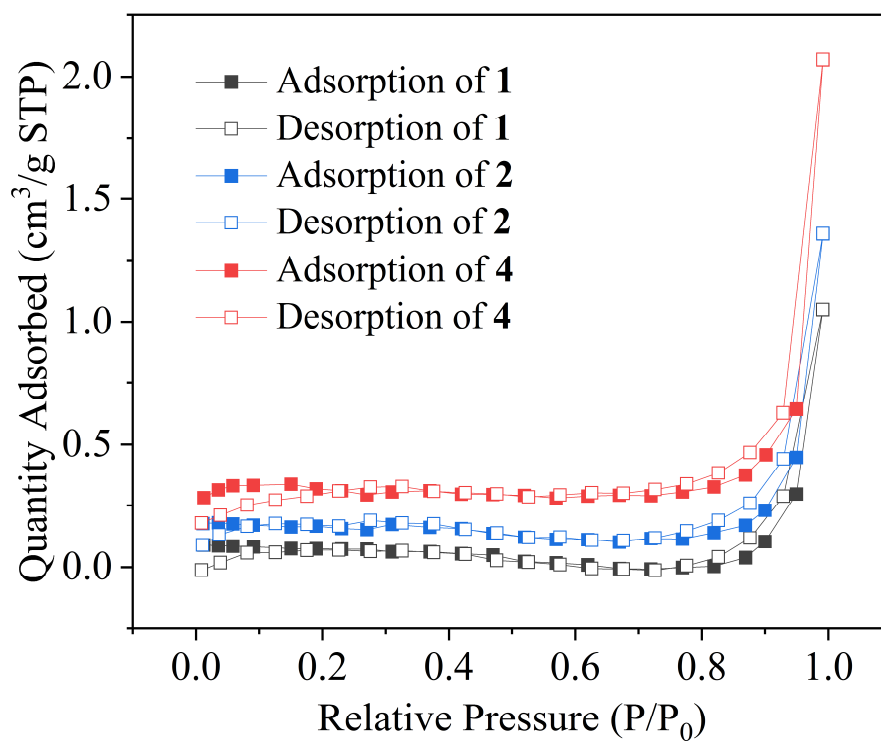


Figure S9. N₂ adsorption-desorption isotherms of (NH₄)₂K₂[V₄(μ₂-OH)₄(ox)₄(pz)₄]·9H₂O (**1**), (NH₄)₂Na₂[V₄(μ₂-OH)₄(ox)₄(4-mpz)₄]·7H₂O (**2**) and [V₈(μ₂-OH)₈(SO₃)₈(Hdatz)₈]·38H₂O (**4**) at 77K.

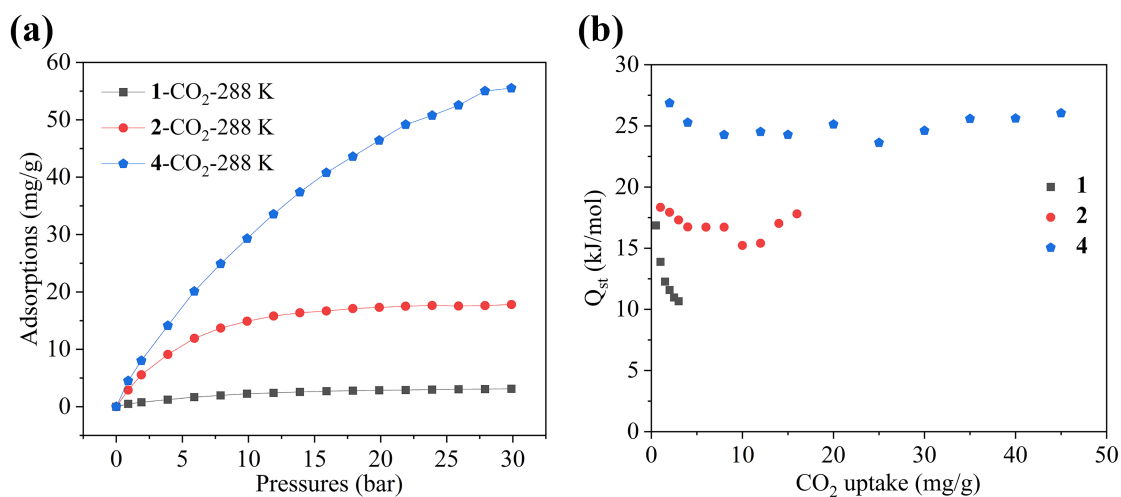


Figure S10. (a) CO₂ adsorption isotherms for **1**, **2** and **4** at 288 K; (b) Isosteric heat of adsorption (Q_{st}) plotted against CO₂ uptake for **1**, **2** and **4**.

Isosteric heat of adsorption was calculated using Clausius–Clapeyron equation:

$$Q_{st} = RT_1T_2 \ln(P_2/P_1)/(T_2 - T_1);$$

$$R = 8.314 \times 10^{-3} \text{ kJ}/(\text{mol} \cdot \text{K}^{-1}), T_1 = 288 \text{ K}, T_2 = 298 \text{ K}.$$

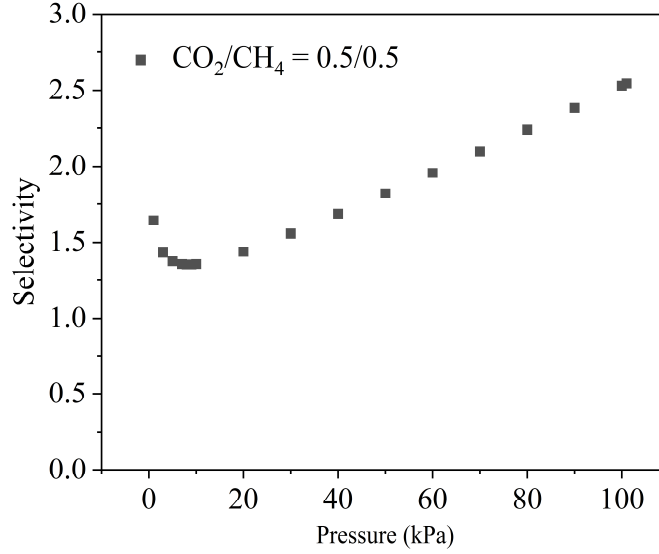


Figure S11. IAST selectivity of equimolar CO₂/CH₄ = 0.5/0.5 mixture for **4**.

Calculation of CO₂/CH₄ selectivity

The ideal adsorbed solution theory (IAST) developed by Myers and Praunitz was used to quantify the CO₂/CH₄ (50/50) selectivities for **4**. Pure component isotherm of CO₂ and CH₄ at 298 K were fitted to the single-site Langmuir-Freundlich (LF) model:

$$N = a \times \frac{bp^c}{1 + bp^c}$$

where a represents the saturation adsorption capacities; b is the affinity constants; p is the pressure of the bulk gas at equilibrium with the adsorbed phase; c is the deviations from an ideal homogeneous surface. The fitting parameters of LF equation as well as the correlation coefficients (R^2) were listed below:

Adsorbates	a	b	c	R^2
CO ₂	3.13	0.02678	0.87785	0.9995
CH ₄	1.04	0.06081	1.04342	0.9990

The adsorption selectivity is defined as

$$S = \frac{x_1 / x_2}{y_1 / y_2}$$

where x is the molar fraction in the adsorbed phase and y is the molar fraction in the gas phase.

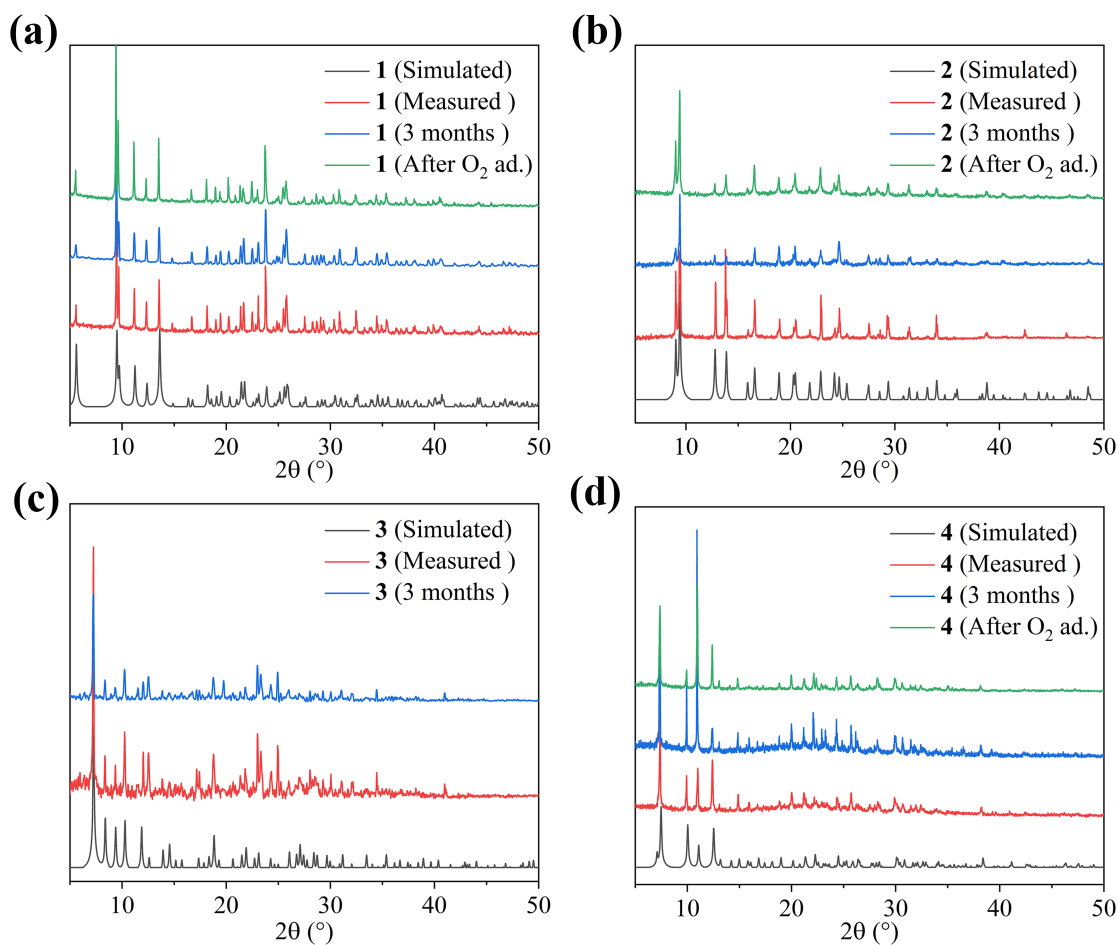


Figure S12. Comparison of the observed PXRD (red) with the simulated patterns (black) calculated from the SXRD data for $(\text{NH}_4)_2\text{K}_2[\text{V}_4(\mu_2\text{-OH})_4(\text{ox})_4(\text{pz})_4]\cdot 9\text{H}_2\text{O}$ (**1**, a), $(\text{NH}_4)_2\text{Na}_2[\text{V}_4(\mu_2\text{-OH})_4(\text{ox})_4(4\text{-mpz})_4]\cdot 7\text{H}_2\text{O}$ (**2**, b), $\text{K}_2[\text{V}_6(\mu_2\text{-OH})_6(\text{ox})_6(\text{Hdatrz})_6]\text{Cl}_2\cdot 29.5\text{H}_2\text{O}$ (**3**, c) and $[\text{V}_8(\mu_2\text{-OH})_8(\text{SO}_3)_8(\text{Hdatrz})_8]\cdot 38\text{H}_2\text{O}$ (**4**, d), respectively.

Table S1. Crystallographic data and structural refinement details for $(\text{NH}_4)_2\text{K}_2[\text{V}_4(\mu_2\text{-OH})_4(\text{ox})_4(\text{pz})_4]\cdot 9\text{H}_2\text{O}$ (**1**), $(\text{NH}_4)_2\text{Na}_2[\text{V}_4(\mu_2\text{-OH})_4(\text{ox})_4(4\text{-mpz})_4]\cdot 7\text{H}_2\text{O}$ (**2**), $\text{K}_2[\text{V}_6(\mu_2\text{-OH})_6(\text{ox})_6(\text{Hdatrz})_6]\text{Cl}_2\cdot 29.5\text{H}_2\text{O}$ (**3**) and $[\text{V}_8(\mu_2\text{-OH})_8(\text{SO}_3)_8(\text{Hdatrz})_8]\cdot 38\text{H}_2\text{O}$ (**4**), respectively.

	1	2	3	4
Empirical formula	$\text{C}_{20}\text{H}_{34}\text{K}_2\text{N}_{10}\text{O}_{29}\text{V}_4$	$\text{C}_{24}\text{H}_{40}\text{N}_{10}\text{Na}_2\text{O}_{27}\text{V}_4$	$\text{C}_{24}\text{Cl}_2\text{H}_{88.5}\text{K}_2\text{N}_{30}\text{O}_{59.5}\text{V}_6$	$\text{C}_{16}\text{H}_{124}\text{N}_{40}\text{O}_{70}\text{S}_8\text{V}_8$
Formula weight	1160.53	1150.40	2204.48	2661.54
Temperature/K	100(1)	100(1)	100(1)	100(1)
Crystal system	Trigonal	Orthorhombic	Cubic	Tetragonal
Space group	$P\ 3_221$	$C\ 222_1$	$P\ a-3$	$P\ 4nc$
$a/\text{\AA}$	18.1163(1)	12.6075(5)	21.0340(1)	17.5495(8)
$b/\text{\AA}$	18.1163(1)	19.6716(6)	21.0340(1)	17.5495(8)
$c/\text{\AA}$	11.4282(6)	19.2268(6)	21.0340(1)	15.9061(1)
$\alpha/^\circ$	90	90	90	90
$\beta/^\circ$	90	90	90	90
$\gamma/^\circ$	120	90	90	90
Volume/ \AA^3	3248.24(4)	4768.40(3)	9306.06(1)	4898.84(6)
Z	3	4	4	2
$\rho_{\text{calc}}/\text{cm}^3$	1.780	1.602	1.573	1.804
μ/mm^{-1}	9.713	7.416	7.211	8.879
$F(000)$	1758.0	2336.0	4514.0	2774.0
Crystal size/ mm^3	$0.10 \times 0.05 \times 0.05$	$0.10 \times 0.05 \times 0.05$	$0.1 \times 0.1 \times 0.05$	$0.1 \times 0.05 \times 0.05$

Radiation	Cu K α ($\lambda = 1.54184$)	Cu K α ($\lambda = 1.54184$)	Cu K α ($\lambda = 1.54184$)	Cu K α ($\lambda = 1.54184$)
2 θ range for data collection/ $^{\circ}$	5.632 to 153.962	8.330 to 133.978	7.280 to 153.388	7.124 to 154.232
Reflections collected	48980	9530	12070	69024
Independent reflections	4498	4005	3071	5037
R_{int}	0.0454	0.0542	0.0259	0.0379
Data/restraints/parameters	4498/2/263	4005/12/291	3071/1/166	5037/6/244
Goodness of fit on F^2	1.040	1.042	1.069	1.039
Final R indexes [$I \geq 2\sigma(I)$]	$R_1 = 0.0472$, $wR_2 = 0.1253$	$R_1 = 0.0736$, $wR_2 = 0.2013$	$R_1 = 0.0524$, $wR_2 = 0.1577$	$R_1 = 0.0477$, $wR_2 = 0.1279$
Final R indexes [all data]	$R_1 = 0.0477$, $wR_2 = 0.1258$	$R_1 = 0.0787$, $wR_2 = 0.2087$	$R_1 = 0.0545$, $wR_2 = 0.1597$	$R_1 = 0.0487$, $wR_2 = 0.1292$
Largest diff. peak and hole / $e\text{\AA}^{-3}$	1.33/-1.07	1.72/-0.50	0.99/-0.32	0.42/-0.58

Table S2. Selected bond distances (Å) and angles (°) for (NH₄)₂K₂[V₄(μ₂-OH)₄(ox)₄(pz)₄]·9H₂O (1), (NH₄)₂Na₂[V₄(μ₂-OH)₄(ox)₄(4-mpz)₄]·7H₂O (2), K₂[V₆(μ₂-OH)₆(ox)₆(Hdatrz)₆]Cl₂·29.5H₂O (3) and [V₈(μ₂-OH)₈(SO₃)₈(Hdatrz)₈]·38H₂O (4), respectively.

1			
V1–O5	1.948(4)	V3–O9	2.041(4)
V1–O6	1.934(4)	V3–N2 ^a	2.081(4)
V1–O1	2.049(4)	V3–N2	2.081(4)
V1–O2	2.043(4)	V2–O6 ^a	1.945(4)
V1–N3	2.105(4)	V2–O6	1.946(4)
V1–N1	2.085(5)	V2–O7 ^a	2.041(7)
V3–O5 ^a	1.947(4)	V2–O7	2.041(7)
V3–O5	1.947(4)	V2–N4	2.097(5)
V3–O9 ^a	2.041(4)	V2–N4 ^a	2.097(5)
O5–V1–O1	88.46(2)	O6 ^a –V2–O6	103.3(2)
O5–V1–O2	163.16(2)	O6–V2–O7	89.5(3)
O5–V1–N3	92.64(2)	O6–V2–O7 ^a	165.5(3)
O5–V1–N1	84.53(2)	O6 ^a –V2–O7	165.5(3)
O6–V1–O5	105.36(2)	O7 ^a –V2–N4 ^a	95.6(3)
O6–V1–O1	164.04(2)	O7–V2–N4 ^a	88.4(3)
O6–V1–O2	90.14(2)	O7 ^a –V2–N4	88.4(3)
O6–V1–N3	84.21(2)	O7–V2–N4	95.6(3)
O6–V1–N1	91.85(2)	N4–V2–N4 ^a	174.9(3)
O1–V1–N3	87.28(2)	O5–V3–O9	91.34(2)
O1–V1–N1	97.47(2)	O5 ^a –V3–O9 ^a	91.34(2)
O2–V1–O1	77.24(2)	O5–V3–O9 ^a	167.24(2)
O2–V1–N3	95.48(2)	O5–V3–N2 ^a	90.99(2)
O2–V1–N1	88.52(2)	O5–V3–N2	84.78(2)
N1–V1–N3	174.38(2)	O5 ^a –V3–N2	91.00(2)
O5 ^a –V3–O5	100.3(2)	O5 ^a –V3–N2 ^a	84.78(2)
O5–V3–O9 ^a	167.24(2)	O9 ^a –V3–O9	77.6(2)
O6 ^a –V2–O7 ^a	89.5(3)	O9–V3–N2	95.33(2)
O6–V2–N4	84.23(2)	O9 ^a –V3–N2	89.81(2)
O6–V2–N4 ^a	92.59(2)	O9–V3–N2 ^a	89.81(2)
O6 ^a –V2–N4 ^a	84.23(2)	O9 ^a –V3–N2 ^a	95.33(2)
O6 ^a –V2–N4	92.59(2)	N2 ^a –V3–N2	173.4(3)
O7–V2–O7 ^a	78.8(6)		

Symmetric codes: (a) $-y + x$, $-y$, $4/3 - z$

2

V1-O10 ^a	1.953(6)	V2-O10	1.955(6)
V1-O5	1.931(6)	V2-O5	1.955(6)
V1-O2	2.036(6)	V2-O7	2.026(6)
V1-O1	2.048(7)	V2-O6	2.061(6)
V1-N4 ^a	2.094(7)	V2-N1	2.100(7)
V1-N2	2.096(7)	V2-N3	2.099(7)

O10 ^a -V1-O2	166.7(3)	O10-V2-O7	89.8(3)
O10 ^a -V1-O1	91.4(3)	O10-V2-O6	165.0(3)
O10 ^a -V1-N4 ^a	85.3(3)	O10-V2-N1	92.0(3)
O10 ^a -V1-N2	91.2(3)	O10-V2-N3	85.1(3)
O5-V1-O10 ^a	101.6(3)	O5-V2-O10	102.0(3)
O5-V1-O2	90.5(3)	O5-V2-O7	166.5(3)
O5-V1-O1	165.5(3)	O5-V2-O6	91.7(3)
O5-V1-N4 ^a	93.0(3)	O5-V2-N1	84.6(3)
O5-V1-N2	85.0(3)	O5-V2-N3	92.1(3)
O2-V1-O1	77.2(3)	O7-V2-O6	77.4(3)
O2-V1-N4 ^a	88.7(3)	O7-V2-N1	88.5(3)
O2-V1-N2	95.30(3)	O7-V2-N3	95.6(3)
O1-V1-N4 ^a	94.4(3)	O6-V2-N1	95.4(3)
O1-V1-N2	88.4(3)	O6-V2-N3	88.3(3)
N4 ^a -V1-N2	175.6(3)	N3-V2-N1	175.0(3)

Symmetric codes: (a) x , $1 - y$, $1 - z$

3

V1-O5	1.934(2)	V1-O1	2.032(2)
V1-O5 ^a	1.938(2)	V1-N2 ^a	2.096(2)
V1-O2	2.038(2)	V1-N1	2.098(2)
O5-V1-O5 ^a	99.66(1)	O5 ^a -V1-N1	89.29(9)
O5 ^a -V1-O2	167.91(8)	O2-V1-N2 ^a	90.78(9)
O5-V1-O2	92.28(8)	O2-V1-N1	93.23(9)
O5-V1-O1	170.18(8)	O1-V1-O2	78.26(9)
O5 ^a -V1-O1	89.90(8)	O1-V1-N2 ^a	92.84(1)
O5 ^a -V1-N2 ^a	87.35(9)	O1-V1-N1	90.69(9)
O5-V1-N2 ^a	89.87(9)	N2 ^a -V1-N1	175.12(1)
O5-V1-N1	87.20(9)		

Symmetric codes: (a) $\frac{1}{2} - y$, $-\frac{1}{2} + z$, x

4

V1-O1	1.944(4)	V2-O1 ^a	1.963(4)
V1-O2	1.969(4)	V2-O2	1.983(4)
V1-O3	2.033(4)	V2-O6	1.986(4)

V1-N1	2.056(5)	V2-O4	2.030(4)
V1-O8 ^b	2.012(4)	V2-N7 ^a	2.159(5)
V1-N6	2.123(5)	V2-N2	2.071(5)
O1-V1-O2	97.84(2)	O1 ^a -V2-O2	91.93(2)
O1-V1-O3	170.21(2)	O1 ^a -V2-O6	90.47(2)
O1-V1-N1	94.61(2)	O1 ^a -V2-O4	172.59(2)
O1-V1-O8 ^b	90.10(2)	O1 ^a -V2-N7 ^a	86.47(2)
O1-V1-N6	84.55(2)	O1 ^a -V2-N2	94.32(2)
O2-V1-O3	87.81(2)	O2-V2-O6	174.50(2)
O2-V1-N1	86.29(2)	O2-V2-O4	89.98(2)
O2-V1-O8 ^b	172.05(2)	O2-V2-N7 ^a	90.95(2)
O2-V1-N6	89.40(2)	O2-V2-N2	85.21(2)
O3-V1-N1	93.70(2)	O6-V2-O4	88.26(2)
O3-V1-N6	87.50(2)	O6-V2-N7 ^a	94.1(2)
N1-V1-N6	175.40(2)	O6-V2-N2	89.7(2)
O8 ^b -V1-O3	84.34(2)	O4-V2-N7 ^a	86.35(2)
O8 ^b -V1-N1	93.00(2)	O4-V2-N2	92.96(2)
O8 ^b -V1-N6	91.50(2)	N2-V2-N7 ^a	176.10(2)

Symmetric codes: (a) $1 - y, x, z$; (b) $y, 1-x, z$

Table S3. Hydrogen bonds observed in $(\text{NH}_4)_2\text{K}_2[\text{V}_4(\mu_2\text{-OH})_4(\text{ox})_4(\text{pz})_4]\cdot 9\text{H}_2\text{O}$ (**1**), $(\text{NH}_4)_2\text{Na}_2[\text{V}_4(\mu_2\text{-OH})_4(\text{ox})_4(4\text{-mpz})_4]\cdot 7\text{H}_2\text{O}$ (**2**), $\text{K}_2[\text{V}_6(\mu_2\text{-OH})_6(\text{ox})_6(\text{Hdatrz})_6]\text{Cl}_2\cdot 29.5\text{H}_2\text{O}$ (**3**) and $[\text{V}_8(\mu_2\text{-OH})_8(\text{SO}_3)_8(\text{Hdatrz})_8]\cdot 38\text{H}_2\text{O}$ (**4**).

D–H⋯A	D–H (Å)	H⋯A (Å)	D⋯A (Å)	D–H⋯A(°)
1				
O5–H5⋯O2w ^a	0.86	1.85	2.710(6)	176
N5–H5B⋯O7	0.91	2.25	2.095(1)	122
N5–H5D⋯O2	0.91	1.83	2.738(1)	179
O6–H6⋯O1w ^b	0.83	1.97	2.773(6)	164
Symmetric codes: (a) $1 - x + y, 1 - x, 1/3 + z$; (b) $y, -1 + x, 1 - z$				
2				
O5–H5⋯N5	0.85(2)	1.87(2)	2.710(1)	170(2)
N5–H5A⋯O8 ^a	0.91	2.03	2.889(2)	156
N5–H5B⋯O3 ^b	0.91	2.42	3.206(2)	145
O10–H10⋯O1w	0.84(4)	1.88(4)	2.689(2)	161(6)
Symmetric codes: (a) $-x, y, 1/2 - z$; (b) $-1/2 + x, 1/2 - y, 1 - z$				
3				
N3–H3⋯O3 ^a	0.88	2.18	2.824(4)	129
N3–H3⋯O4 ^a	0.88	2.14	2.880(4)	141
N4–H4A⋯O1	0.88	2.22	2.946(4)	140
N4–H4B⋯O3 ^a	0.88	2.34	2.985(4)	130
O5–H5⋯Cl1	0.85(3)	2.31(4)	3.150(2)	169(4)

N5–H5A···O2	0.88	2.32	3.022(4)	137
N5–H5B···O4 ^a	0.88	2.37	3.089(4)	140

Symmetric codes: (a) $1 - y, 1 - z, 1 - x$

4

N3–H3···O5 ^a	0.88	1.85	2.694(7)	160
N4–H4A···O7 ^b	0.88	2.39	3.192(9)	152
N4–H4A···O8 ^b	0.88	2.34	3.048(9)	137
N5–H5B···O6	0.89	2.12	2.938(8)	152
N9–H9A···O3	0.88	2.57	3.119(9)	121
N10–H10A···O4 ^b	0.88	2.19	2.919(8)	140

Symmetric codes: (a) $-\frac{1}{2} + y, \frac{1}{2} + x, \frac{1}{2} + z$; (b) $y, 1 - x, z$

Table S4. Comparisons of V–O distances (Å) in **1** ~ **4** and a series of tetra-, hexa- and octanuclear vanadium(III/IV/V) clusters with bridging μ_2 -hydroxy/ μ_2 -oxygen groups.

Complexes	V– μ_2 -OH	V– μ_2 -O
{V^V₄O₁₂}		
[Co ₂ (phen) ₄ V ₄ O ₁₂] C ₆ H ₁₁ OH·H ₂ O ¹		1.791(3)
[Mn ₂ (phen) ₄ V ₄ O ₁₂] C ₆ H ₁₁ OH·H ₂ O ¹		1.788(4)
[Ni ₂ (phen) ₄ V ₄ O ₁₂] C ₆ H ₁₁ OH·H ₂ O ¹		1.794(4)
[{Ni(quarterpy)(H ₂ O)} ₂ V ₄ O ₁₂] 10H ₂ O ²		1.778(4)
Average		1.788(4)
{V^V₄O₈}		
Na ₄ [V ₄ O ₈ (<i>rac</i> -tart) ₂] 12H ₂ O ³		1.826(2)
(NEt ₄) ₄ [V ₄ O ₈ ((<i>R,R</i>)-tart) ₂] 6H ₂ O ³		1.832(2)
(C ₂₄ H ₂₀ P)[V ₄ O ₈ (C ₂ H ₃ O ₂) ₄ (NO ₃) ₄] ⁴		1.811(2)
Average		1.823(2)
{V^V₆O₁₃}		
(Bu ₄ N) ₂ [V ₆ O ₁₃ {(OCH ₂) ₃ CCH ₂ OOCC ₆ H ₄ Br- <i>p</i> } ₂] ⁵		1.835(3)
(Bu ₄ N) ₂ [V ₆ O ₁₃ {(OCH ₂) ₃ CCH ₂ OOCC ₆ H ₄ NO ₂ - <i>m</i> } ₂] ⁵		1.841(5)
(Bu ₄ N) ₂ [V ₆ O ₁₃ {(OCH ₂) ₃ CCH ₂ OOCC ₄ H ₃ S} ₂] ⁵		1.843(2)
Average		1.840(5)
{V^{IV}₄O₄}		
[Cp*VCl(μ -O)] ₄ ⁶		1.800(2)
{V^{III}₄(OH)₄}		
(NH ₄) ₂ K ₂ [V ₄ (μ_2 -OH) ₄ (ox) ₄ (pz) ₄]·9H ₂ O (1)	1.942(5)	
(NH ₄) ₂ Na ₂ [V ₄ (μ_2 -OH) ₄ (ox) ₄ (4-mpz) ₄]·7H ₂ O (2)	1.939(5)	
[V ₄ (μ -OOCCH ₃) ₄ (μ -OH) ₄ (OH ₂) ₈]Cl ₄ ·3H ₂ O ⁷	1.939(1)	
[V ₄ (μ -OH) ₄ (μ -OOCF ₃) ₄ (OH ₂) ₈]Cl ₄ ·7.5H ₂ O ⁸	1.939(3)	
[V ₄ (μ -OH) ₄ (μ -OOCCH ₃) ₄ (OH ₂) ₈]Cl ₄ ·CH ₃ COOH·12H ₂ O ⁸	1.939(1)	
[V ₄ (μ -OH) ₄ (μ -OOCCH ₃) ₄ (OH ₂) ₈]Cl ₄ ·3H ₂ O ⁸	1.940(4)	
Average	1.940(5)	
{V^{III}₄O₂}		

[{V(μ -hpnbpda) ₂ } { μ -(C ₆ H ₅ O) ₂ PO ₂ } ₂ (μ -O) ₂].6CH ₃ OH ⁹ {V^{III}₆(OH)₆}	1.897(5)
K ₂ [V ₆ (μ ₂ -OH) ₆ (ox) ₆ (Hdatrz) ₆]Cl ₂ ·29.5H ₂ O (3) {V^{III}₈(OH)₈}	1.936(2)
[V ₈ (μ ₂ -OH) ₈ (SO ₃) ₈ (Hdatrz) ₈]·38H ₂ O (4)	1.965(4)
D-[H ₂ N(CH ₃) ₂] _{12.5} (H ₃ N(CH ₂) ₂ NH ₃)(H ₃ O) _{1.5} (V μ ₂ -OH) ₈ (SO ₄) ₁₆ ·2H ₂ O ¹⁰	1.957(3)
L-[H ₂ N(CH ₃) ₂] _{12.5} (H ₃ N(CH ₂) ₂ NH ₃)(H ₃ O) _{1.5} (V μ ₂ -OH) ₈ (SO ₄) ₁₆ ·2H ₂ O ¹⁰	1.966(5)
[(CH ₃) ₂ NH ₂] _{17.4} [V ₈ (μ ₂ -OH) ₈ (μ ₂ -SO ₄) ₁₆][SO ₄] _{0.7} ¹¹	1.949(2)
[V ₈ (μ -OH) ₄ (μ -OEt) ₈ (μ -CH ₃ COO) ₁₂] ¹²	1.967(7)
Average	1.961(7)

Table S5. Bond valence sum calculations for $(\text{NH}_4)_2\text{K}_2[\text{V}_4(\mu_2\text{-OH})_4(\text{ox})_4(\text{pz})_4]\cdot 9\text{H}_2\text{O}$ (**1**), $(\text{NH}_4)_2\text{Na}_2[\text{V}_4(\mu_2\text{-OH})_4(\text{ox})_4(4\text{-mpz})_4]\cdot 7\text{H}_2\text{O}$ (**2**), $\text{K}_2[\text{V}_6(\mu_2\text{-OH})_6(\text{ox})_6(\text{Hdatrz})_6]\text{Cl}_2\cdot 29.5\text{H}_2\text{O}$ (**3**) and $[\text{V}_8(\mu_2\text{-OH})_8(\text{SO}_3)_8(\text{Hdatrz})_8]\cdot 38\text{H}_2\text{O}$ (**4**), respectively.

Complexes	Atoms	n	s	d	Assignment
1	V(1)	3	2.986	0.014	
	V(2)	3	2.982	0.018	
	V(3)	3	3.017	0.017	
	average	3	2.995	0.005	V(III)
	O(5)	1	1.194	0.194	$\mu_2\text{-OH}^-$
	O(6)	1	1.170	0.170	$\mu_2\text{-OH}^-$
2	V(1)	3	2.994	0.006	
	V(2)	3	2.937	0.063	
	average	3	2.966	0.034	V(III)
	O(5)	1	1.184	0.184	$\mu_2\text{-OH}^-$
	O(10)	1	1.149	0.149	$\mu_2\text{-OH}^-$
3	V(1)	3	3.025	0.025	V(III)
	O(5)	1	1.208	0.208	$\mu_2\text{-OH}^-$
4	V(1)	3	3.015	0.015	
	V(2)	3	2.941	0.059	
	average	3	2.978	0.022	V(III)
	O(3)	1	1.151	0.151	$\mu_2\text{-OH}^-$
	O(4)	1	1.083	0.083	$\mu_2\text{-OH}^-$

Table S6. Comparisons of CO₂ adsorption data for **1**, **2** and **4** with other porous polyoxometalates at 298 K.

Adsorbents	Amount (mmol·g ⁻¹)	Pressure (bar)
1	0.006	1
2	0.053	1
4	0.089	1
	1.080	30
[Mo ^V ₈ O ₈ (μ ₂ -O) ₁₂ (Htrz) ₈]·62H ₂ O ¹³	0.052	1
Na ₃ [Mo ^V ₆ O ₆ (μ ₂ -O) ₉ (Htrz) ₃ (trz) ₃]·7.5H ₂ O ¹⁴	0.020	1
COMOC-2 ¹⁵	1.230	1
SO ₂ -COMOC-2 ¹⁵	2.130	1
MFM-300(V ^{III}) ¹⁶	6.000	1
MFM-300(V ^{IV}) ¹⁶	3.540	1
NH ₂ -MIL-47 ¹⁷	5.800	29
V-MIL-100 ¹⁸	14.2	1

Abbreviations: Htrz = 1H-1,2,3-triazole; SO₂-COMOC-2 = [V^{III}(O)V^{IV}(OH)(C₁₄H₆SO₆)₂]-
(DMF)_{0.3}(H₂O)_{0.7}(CH₃OH)_{1.15}; MFM-300(V^{III}) = V^{III}₂(OH)₂(biphenyl-3,3',5,5'-
tetracarboxylate); MFM-300(V^{IV}) = V^{IV}₂O₂(biphenyl-3,3',5,5'-tetracarboxylate).

Table S7. V- μ_2 -O distances (\AA) for $(\text{NH}_4)_2\text{K}_2[\text{V}_4(\mu_2\text{-OH})_4(\text{ox})_4(\text{pz})_4]\cdot 9\text{H}_2\text{O}$ (**1**), $(\text{NH}_4)_2\text{Na}_2[\text{V}_4(\mu_2\text{-OH})_4(\text{ox})_4(4\text{-mpz})_4]\cdot 7\text{H}_2\text{O}$ (**2**) and $[\text{V}_8(\mu_2\text{-OH})_8(\text{SO}_3)_8(\text{Hdatrz})_8]\cdot 38\text{H}_2\text{O}$ (**4**) before and after O_2 adsorption.

Before O_2 adsorption			After O_2 adsorption		
1	V1-O5	1.948(4)	1	V1-O5	1.940(5)
	V1-O6	1.934(4)		V1-O6	1.932(5)
	V2-O6	1.946(4)		V2-O6	1.947(5)
	V3-O5	1.947(4)		V3-O5	1.949(5)
2	V1-O5	1.931(6)	2	V1-O5	1.926(2)
	V2-O5	1.955(6)		V2-O5	1.949(2)
	V2-O10	1.955(6)		V2-O10	1.941(2)
4	V1-O1	1.944(4)	4	V1-O1	1.939(4)
	V1-O2	1.969(4)		V1-O2	1.951(4)
	V2-O2	1.983(4)		V2-O2	1.980(4)

References

1. V. Paredes-García, S. Gaune, M. Saldías, M. T. Garland, R. Baggio, A. Vega, M. S. El Fallah, A. Escuer, E. L. Fur, D. Venegas-Yazigi and E. Spodine, *Inorg. Chim. Acta.*, 2008, **361**, 3681–3689.
2. D. Xiao, Y. Hou, E. Wang, J. Lü, Y. Li, L. Xu and C. Hu, *Inorg. Chem. Commun.*, 2004, **7**, 437–439.
3. P. Schwendt, A. S. Tracey, J. Tatiarsky, J. Gálíková and Z. Žák, *Inorg. Chem.*, 2007, **46**, 3971–3983.
4. D. Wulff-Molder and M. Meisel, *Acta Cryst. C*, 2000, **56**, 33–34.
5. B. Huang, M. Cheng, J. Cai, B. Wu, W. Xiong, X. Hu, Z. Xiao and P. Wu, *J. Chem. Crystallogr.*, 2017, **47**, 95–100.
6. F. Bottomley, J. Darkwa, L. Sutin and P. S. White, *Organometallics*, 1986, **5**, 2165–2171.
7. F. H. Fry, B. A. Dougan, N. McCann, C. J. Ziegler and N. E. Brasch, *Inorg. Chem.*, 2005, **44**, 5197–5199.
8. R. Mukherjee, B. A. Dougan, F. H. Fry, S. D. Bunge, C. J. Ziegler and N. E. Brasch, *Inorg. Chem.*, 2007, **46**, 1575–1585.
9. K. Sato, T. Ohnuki, H. Takahashi, Y. Miyashita, K. Nozaki and K. Kanamori, *Inorg. Chem.*, 2012, **51**, 5026–5036.
10. J. P. Cao, Y. S. Xue, Z. B. Hu, X. M. Luo, C. H. Cui, Y. Song and Y. Xu, *Inorg. Chem.*, 2019, **58**, 2645–2651.
11. M. G. Sorolla, X. Q. Wang, T. Makarenko and A. J. Jacobson, *Chem. Commun.*, 2019, **55**, 342–344.
12. R. H. Laye, M. Murrie, S. Ochsenbein, A. R. Bell, S. J. Teat, J. Raftery, H. U. Gudel and E. J. L. McInnes, *Chem. Eur. J.*, 2003, **9**, 6215–6220.
13. L. Deng, R. Y. Lin and Z. H. Zhou, *Dalton Trans.*, 2022, **51**, 5239–5249.
14. L. Deng, X. Dong and Z. H. Zhou, *Chem. Eur. J.*, 2021, **27**, 9643–9653.
15. G. Wang, K. Leus, S. Couck, P. Tack, H. Depauw, Y. Y. Liu, L. Vincze, J. F. M. Denayer and P. Van Der Voort, *Dalton Trans.*, 2016, **45**, 9485–9491.
16. Z. Z. Lu, H. G. W. Godfrey, I. da Silva, Y. Q. Cheng, M. Savage, F. Tuna, E. J. L. McInnes, S. J. Teat, K. J. Gagnon, M. D. Frogley, P. Manuel, S. Rudic, A. J. Ramirez-Cuesta, T. L. Easun, S. H. Yang and M. Schroder, *Nat. Commun.*, 2017, **8**, 14212.
17. K. Leus, S. Couck, M. Vandichel, G. Vanhaelewyn, Y. Y. Liu, G. B. Marin, I. Van Driessche, D. Depla, M. Waroquier, V. Van Speybroeck, J. F. M. Denayer and P. Van Der Voort, *Phys. Chem. Chem. Phys.*, 2012, **14**, 15562–15570.
18. A. Lieb, H. Leclerc, T. Devic, C. Serre, I. Margiolaki, F. Mahjoubi, J. S. Lee, A. Vimont, M. Daturi and J. S. Chang, *Micropor. Mesopor. Mater.*, 2012, **157**, 18–23.